REPORT DOCUMENTATION PAGE

Form Approved
OMB No. 0704-0188

1. REPORT DATE *(DD-MM-YYYY)*	**2. REPORT TYPE**	**3. DATES COVERED** *(From - To)*
28-06-1999	Technical Paper	

4. TITLE AND SUBTITLE

Laser-Induced Fluorescence Measurements within a Laboratory Hall Thruster (Postprint)

5a. CONTRACT NUMBER

5b. GRANT NUMBER

5c. PROGRAM ELEMENT NUMBER

6. AUTHOR(S)
W. A. Hargus, Jr. and M.A. Cappelli (Stanford Univ.)

5d. PROJECT NUMBER

5e. TASK NUMBER

5f. WORK UNIT NUMBER

7. PERFORMING ORGANIZATION NAME(S) AND ADDRESS(ES)

Air Force Research Laboratory (AFMC)
AFRL/PRSS
1 Ara Road.
Edwards AFB CA 93524-7013

8. PERFORMING ORGANIZATION REPORT NUMBER

AIAA-99-3436

9. SPONSORING / MONITORING AGENCY NAME(S) AND ADDRESS(ES)

Air Force Research Laboratory (AFMC)
AFRL/PRSS
1 Ara Road
Edwards AFB CA 93524-7013

10. SPONSOR/MONITOR'S ACRONYM(S)

11. SPONSOR/MONITOR'S NUMBER(S)
AIAA-99-3436

12. DISTRIBUTION / AVAILABILITY STATEMENT

Approved for public release; distribution unlimited.

13. SUPPLEMENTARY NOTES
Presented at the 30th Plasmadynamics and Lasers Conference, 28 June – 1 July 1999, Norfolk, VA. AIAA-99-3436.

14. ABSTRACT

In this paper, we describe the results of a study of laser induced fluorescence velocimetry of ionic xenon in the plume and interior acceleration channel of a laboratory Hall type thruster operating at powers ranging from 250 to 725 W. Optical access to the interior of the Hall thruster is provided by a 1 mm axial slot in the insulator outer wall. Axial ion velocity profiles for four discharge voltages (100 V, 160 V, 200 V, 250 V) are measured as are radial velocity profiles in the near field plume. Internal neutral xenon axial velocity profiles are also measured at these conditions. For each test condition, the implied axial electric field is calculated from the measured ionic velocity profiles. These results are compared to previous plasma potential measurements performed with an emissive probe. The correspondence between the two sets of measurements indicates that the ionization and acceleration regions within the thruster are separated to some degree.

15. SUBJECT TERMS

16. SECURITY CLASSIFICATION OF:			**17. LIMITATION OF ABSTRACT**	**18. NUMBER OF PAGES**	**19a. NAME OF RESPONSIBLE PERSON**
					Dr. William A. Hargus, Jr.
a. REPORT	**b. ABSTRACT**	**c. THIS PAGE**	SAR	15	**19b. TELEPHONE NUMBER** *(include area code)*
Unclassified	**Unclassified**	**Unclassified**			N/A

A99-33770

AIAA-99-3436

Laser-Induced Fluorescence Measurements within a Laboratory Hall Thruster

W.A. Hargus, Jr. and M.A. Cappelli
Mechanical Engineering Department
Thermosciences Division
Stanford University
Stanford, CA 94305

30th Plasmadynamics and Lasers Conference
28 June - 1 July, 1999 / Norfolk, VA

Laser Induced Fluorescence Measurements within a Laboratory Hall Thruster

W.A. Hargus, Jr.* and M.A. Cappelli
Mechanical Engineering Department
Thermosciences Division
Stanford University
Stanford, CA 94305

Abstract

In this paper, we describe the results of a study of laser induced fluorescence velocimetry of ionic xenon in the plume and interior acceleration channel of a laboratory Hall type thruster operating at powers ranging from 250 to 725 W. Optical access to the interior of the Hall thruster is provided by a 1 mm axial slot in the insulator outer wall. Axial ion velocity profiles for four discharge voltages (100 V, 160 V, 200 V, 250 V) are measured as are radial velocity profiles in the near field plume. Internal neutral xenon axial velocity profiles are also measured at these conditions. For each test condition, the implied axial electric field is calculated from the measured ionic velocity profiles. These results are compared to previous plasma potential measurements performed with an emissive probe. The correspondence between the two sets of measurements indicates that the ionization and acceleration regions within the thruster are separated to some degree.

Introduction

Due to their high specific impulse and high thrust efficiencies, Hall thrusters are now being considered for use on commercial, research, and military spacecraft. This technology provides economic advantages for a number of missions and its use can be translated into lower launch mass, longer time on station, or larger payloads [1].

There is a need for increased understanding of the complex phenomena that govern the operation of Hall thrusters. In order to more fully understand the physics in these discharges, several laboratory model Hall thrusters have been constructed at Stanford University. These thrusters have served as test articles for model development and advanced plasma diagnostics including laser induced fluorescence (LIF), probes of various types, and thrust measurements [2-8].

Laser based techniques have been developed to nonintrusively probe neutral and ionized xenon [6-8]. Such measurements in the plumes of Hall and other types of ion thrusters provide information on the plasma discharge that is useful in developing insight into the physical processes occurring within these devices. Similar optical diagnostic measurements have been previously employed to examine plasma properties in other electric propulsion devices. For example, the hydrogen arcjet has been extensively studied using lasers to measure velocity, temperature, and electron number density [9]. The high spatial resolution of single point laser-induced fluorescence is essential in probing nonuniform plasma environments such as those in Hall thrusters and other electric propulsion devices.

Theory

Laser Induced Fluorescence

The interaction of a laser beam with a plasma may involve the optical excitation of a number of atoms to a higher energy state. The excitation is more likely to occur if the laser is tuned to the energy difference $h\nu_{12}$ between an upper and lower excitation level. The interaction can be investigated by either monitoring the resulting reduction in laser power following propagation through the plasma (absorption process), or by monitoring the subsequent spontaneous emission as the resulting excited state relaxes to a lower state (laser-induced fluorescence, LIF). Monitoring the fluorescence as the laser is tuned over the transition provides a measure of the fluorescence excitation line shape and is favored for the higher spatial resolution that it affords in the determination of plasma parameters.

* Now located at
Air Force Research Laboratory
Spacecraft Propulsion Branch
Edwards AFB, CA

The spatial resolution for LIF is determined by the intersection of the probe laser beam with the optical collection volume.

If an absorber has a velocity component u along the axis of the laser beam, it will absorb the light at a frequency shifted from that of stationary absorbers due to the Doppler effect. The magnitude of this frequency shift depends on the velocity along the laser beam axis by,

$$\delta\nu_{12} = \nu_{12}\frac{u}{c} \qquad (1)$$

where c is the speed of light. The Doppler shift of a species' fluorescence profile away from the line center ν_{12} of stationary absorbers is in proportion to the species bulk velocity.

The measured fluorescence signal is given by [10-12]

$$S_f = \eta_d \alpha_c h\nu_{12} A_{21} N_2 \qquad (2)$$

where η_{12} is the efficiency of the detection system, α_c accounts for factors involving the collection system, and A_{21} is the Einstein coefficient for spontaneous emission of the relevant transition. For low laser intensities, rate equation analysis indicates that the upper level population N_2, and therefore the fluorescence signal, is linearly dependent on laser intensity at steady state, i.e.,

$$N_2 \sim I_\nu B_{12} \phi_\nu \qquad (3)$$

where I_ν is the spectral irradiance at frequency ν, B_{12} is the Einstein stimulated absorption coefficient, and ϕ_ν is the transition's spectral line shape which accounts for the variation of the absorption or laser excitation with frequency. The line shape is determined by the environment of the absorbing atoms, so an accurate measurement of the line shape function can lead to the determination of various plasma parameters. However, for velocity measurements, partially saturated fluorescence with a distorted line shape is still capable of providing a reasonable measure of the mean ion velocity. This was experimentally verified with two saturation studies which also determined velocity. The variation of the velocities were found to be less than the experimental uncertainty for the ions (±500 m/s), or for the neutrals (±60 m/s).

Several factors can affect the line shape and give rise to a broadening and/or shift of the spectral line. In high temperature plasmas, the most significant of these is due to the Doppler effect and gives rise to Doppler broadening. Doppler broadening reflects the fact that the absorbing species is distributed in velocity according to the kinetic temperature, T_{kin}. When the absorbing species is characterized by a Maxwellian velocity distribution, Doppler broadening results in a Gaussian line shape. Collisional interactions between the absorbers and other species in the plasma give rise to spectral line shapes that are often Lorentzian. This includes interactions with charged particles (Stark broadening) and uncharged particles (van der Waals broadening). If both Doppler broadening and collision broadening are important and independent, the resulting line shape is a convolution of the Gaussian and Lorentzian line shape into a Voigt line shape [12].

The line shape is an intrinsic property of the absorbers, whereas the fluorescence excitation line shape is the variation in the detected fluorescence signal with frequency as the laser is tuned across the absorption line feature. If the laser excitation significantly perturbs the populations in the coupled levels, it is said to be saturating the transition and the fluorescence signal is then a nonlinear function of laser intensity. In cases where the laser intensity is significantly below the saturation level and the laser linewidth is small compared to the measured linewidth, the fluorescence excitation line shape reflects the spectral absorption line shape as given by Eqns. 2 and 3. When the laser intensity is sufficiently high to saturate the transition, the fluorescence excitation line shape is broader than the spectral line shape and the fluorescence intensity is less than it would be if it were linear with the laser intensity I_ν. The saturation intensity, defined as that intensity which produces a fluorescence signal half of what it would be if the fluorescence was linear with I_ν, depends inversely on the line strength of the particular line. Stronger transitions have a smaller saturation intensity and thus a larger saturation effect for a given laser intensity.

Hyperfine Structure

The seven xenon isotopes each have a slight difference in their transition energies due to their differences in mass. The odd mass isotopes are further spin split due to nuclear magnetic dipole and nuclear electric quadrapole moments [13].

Many nuclei which have an odd number of protons and/or an odd number of neutrons posses an intrinsic nuclear spin $Ih/2\pi$. Where I is integral, or half-integral, dependent on if the atomic mass is even or odd, respectively [14]. For nuclei with nuclear spin, there exists an interaction of the nucleus with the electron shell. The interaction leads to the splitting of levels with angular momentum **J** into a number of components, each corresponding a specific value of the total angular momentum **F** [15].

$$\mathbf{F} = \mathbf{I} + \mathbf{J} \tag{4}$$

As a result of this interaction, **F** is a conserved quantity while **I** and **J** are not. The interaction is very small allowing the hyperfine splitting of each level to be taken independently of the other levels. The number of nuclear spin split hyperfine components is $2I + 1$ if $J \geq I$ and $2J + 1$ if $J < I$ with F values shown below [15,16].

$$F = J + I, J + I - 1, \ldots, |J - I| \tag{5}$$

In turn, the selection rules for F are given below.

$$\Delta F = 0, \pm 1 \tag{6}$$

$$\Delta F \neq 0, \text{ if } F = 0 \tag{7}$$

Two constants are associated with hyperfine nuclear spin splitting. These are the A hyperfine structure constant which represents the nuclear magnetic dipole effect on the atom, and the B hyperfine structure constant which is associated with the nuclear electric quadrapole moment of the atom which will only be present if $I \geq 1$. The relative energy of the spin split states depends on the sign of A. In atoms with $A > 0$, the state with the highest value of F has the highest energy, while for atoms with $A < 0$, the state with the lowest value of F has the highest energy [16]. The energy level shift ΔE_M associated with the magnetic dipole of the nucleus is given by [14]

$$\Delta E_M(F) = \frac{1}{2}A[F(F+1) - J(J+1) - I(I+1)] = \frac{A}{2}C \tag{8}$$

Additionally, the energy spacing between successive levels $F-1$ and F may be shown to be proportional to F.

$$\Delta E_M(F) - \Delta E_M(F-1) = AF \tag{9}$$

If $I \geq 1$, the nucleus will have an electric quadrapole moment and a related hyperfine splitting constant B which produces an additional hyperfine splitting with energy linear in $C(C+1)$ where C is defined in Eqn. 8.

$$\Delta E_F = \Delta E_M + \Delta E_Q = \frac{AC}{2} + B\left[C(C+1) - \frac{4}{3}J(J+1)I(I+1)\right] \tag{10}$$

Where ΔE_F is the combined nuclear spin split energy level shift combining the effect from the nuclear magnetic dipole moment, ΔE_M, and the effect of the electric quadrapole moment, ΔE_Q [14]. It should be noted that the center of gravity of the hyperfine levels lies at a position of the unsplit level J [15].

$$\sum_F (2F+1)\Delta E_F = 0 \tag{11}$$

Due to close energy spacing of nuclear spin split levels, near ideal coupling between **I** and **J** occurs in most hyperfine structure. Therefore, the relative intensity rules derived in the literature for Russel-Saunders coupling are appropriate for hyperfine splitting [16].

For where $J - 1 \rightarrow J$,

$F - 1 \rightarrow F$:

$$\frac{(J+F+I+1)(J+F+I)(J+F-I)(J+F-I-1)}{F}$$

$F \rightarrow F$:

$$\frac{(J+F+I+1)(J+F-I)(J-F+I)(J-F-I-1)(2F+1)}{F(F+1)}$$

$F + 1 \rightarrow F$:

$$\frac{(J-F+I)(J-F+I-1)(J-F-I-1)(J-F-I-2)}{(F+1)}$$

For where $J \rightarrow J$,

$F - 1 \rightarrow F$:

$$\frac{(J+F+I+1)(J+F-I)(J-F+I+1)(J-F-I)}{F}$$

$F \rightarrow F$:

$$\frac{[J(J+1) + F(F+1) + I(I+1)]^2(2F+1)}{F(F+1)}$$

$F + 1 \rightarrow F$:

$$\frac{(J+F+I-2)(J+F-I+1)(J-F+I)(J-F-I-1)}{(F+1)} \quad (12)$$

The relative intensities of the isotope shifted transitions are proportional to each isotope's relative abundance shown in Table 1. The relative intensities of the nuclear spin split hyperfine splitting are governed by two summation rules [15]. First, the sum of the intensities all the lines of the hyperfine structure of a transition $J \rightarrow J'$ originating from a component F of the level J is proportional to the statistical weight of this component, $2F+1$. Second, the sum of the intensities of all the lines of the hyperfine structure the transition $J \rightarrow J'$ ending on the component F' of the level J' is proportional to the statistical weight of this component, $(2F'+1)$. With these two sum rules, a system of linear equations are solved for the relative intensities of the nuclear spin split components of each isotope.

Xenon Spectroscopy

The isotopic and nuclear-spin effects contributing to the hyperfine structure of the $6s[3/2]_2^0 - 6p[3/2]_2$ neutral xenon transition at 823.2 nm produce 21 individual lines. Similarly, the $5d[4]_{7/2} - 6p[3]_{5/2}$ ionic xenon transition at 834.7 nm shown in Fig. 1 has a total of 19 isotopic and spin split components. The hyperfine splitting constants are only known for a limited set of levels several of which are shown in Table 2. The neutral 823.2 nm transition has all of these measured and tabulated in the literature. The ionic 834.7 nm transition only has data on the nuclear spin splitting of the upper state and no available information on the transition dependent isotope shifts.

For LIF measurements primarily aimed at determining velocities within the plasma flow, it is often convenient to probe more accessible transitions for which there is incomplete knowledge of the isotopic and nuclear spin splitting constants.

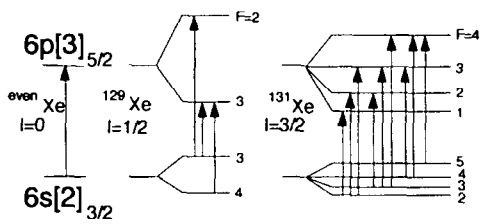

Fig. 1. Nuclear spin splitting of the $5d[4]_{7/2} - 6p[3]_{5/2}$ transition of singly ionized xenon at 834.7 nm.

Manzella has shown that the ionic xenon transition at 834.7 nm can be used to make velocity measurements in the plume of a Hall thruster [17,18]. An additional convenient feature of this transition is a strong line emanating from the same upper state. This transition at 541.9 nm allows for nonresonant fluorescence collection.

Table 1: Xenon natural isotope abundances, nuclear spins, and representative isotope shifts for Xe I and Xe II transitions relative to ^{132}Xe in MHz [14,19-20].

	% Natural Abundance	Nuclear Spin	Xe I 823.2nm Isotope Shift	Xe II 605.1nm Isotope Shift
^{124}Xe	0.10	0	270 ± 12	336.6 ± 3.9
^{126}Xe	0.09	0	189 ± 12	252.4 ± 3.9
^{128}Xe	1.91	0	117 ± 12	172.0 ± 6.8
^{129}Xe	26.4	1/2	123 ± 18	113.7 ± 5.0
^{130}Xe	4.1	0	54 ± 12	83.6 ± 4.5
^{131}Xe	21.2	3/2	81 ± 18	16.7 ± 5.0
^{132}Xe	26.9	0	0	0
^{134}Xe	10.4	0	-30 ± 12	-75.8 ± 4.0
^{136}Xe	8.9	0	-147 ± 12	-140.9 ± 7.3

Table 2: Hyperfine spin splitting constants for Xe I and Xe II in MHz [23-25].

	State	A_{129}	A_{131}	B_{131}
Xe I	$6s[3/2]_2^0$	-2384 ± 2	707 ± 1	525 ± 2
Xe I	$6p[3/2]_2$	887 ± 1	265 ± 3	30 ± 3
Xe II	$5d[3]_{7/2}$	-502 ± 4	150 ± 2	70 ± 13
Xe II	$6p[2]_{5/2}$	-1633 ± 11	487 ± 4	-129 ± 16
Xe II	$6p[3]_{7/2}$	-1387 ± 9	409 ± 2	-117 ± 10
Xe II	$6p[3]_{5/2}$	-1164 ± 5	346 ± 2	-230 ± 11

Test Apparatus

Hall Thruster

The thruster used in this study has been described extensively elsewhere [7]. It has 4 outer magnetic windings consisting of 89 mm long, 25 mm diameter cores of commercially pure iron wrapped with 6 layers of 22 gauge insulated copper magnet wire. The inner core is also 25 mm in diameter and 89 mm in height and has 12 layers of magnet wire. The depth of the electrical insulator is 84 mm. The insulator is constructed from 2 sections of cast 99.9% alumina tubing cut to length. These two pieces are cemented to a machinable alumina plate attached to the back plate of the thruster with nonconducting fasteners. A photograph of the assembled thruster is shown in Fig. 2.

A second insulator was constructed for the modified Hall thruster. It is identical to the insulator described above with a slot approximately 1 mm wide along the length of the outer wall of cast alumina cut with a diamond saw prior to assembly. The slot is used to provide optical access to the interior of the Hall thruster. Operation of the Hall thruster with the slotted insulator does not appear to differ significantly from the operation with the unslotted insulator. The current voltage characteristics are identical and there are no apparent differences in thruster operation. A photograph of the slotted insulator is also shown in Fig. 2. Here, the insulator is shown after testing has been completed. The dark deposits on the insulator are the result of the partial carbonization of the phenolic thruster mount.

The optical access provided by the slot is blocked near the exit plane by the front plate of the magnetic circuit. The front plate is not cut since this would modify the local magnetic field. The magnetic field is one of the most important parameters determining the behavior of the plasma in the Hall thruster and any change in the field would immediately change the characteristics of the plasma. It is felt that the 4 mm field of view blocked by the front plate of the magnetic circuit is less important than preserving the uniformity of the magnetic field within the Hall thruster.

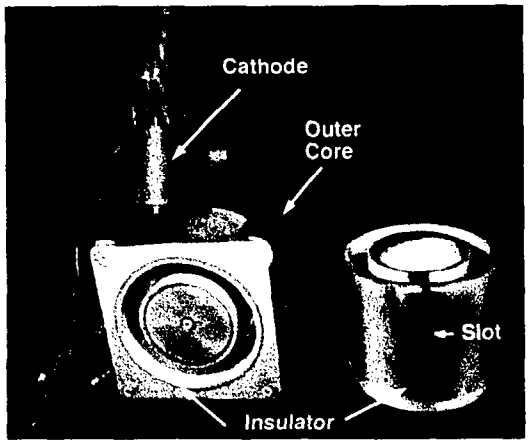

Fig. 2. Photograph of Hall thruster with slotted insulator beside it.

The thruster is mounted on a two axis translation system. In the vertical, the thruster has a range of travel of approximately 30 cm. In the axial, or horizontal, direction, the thruster is constrained to a total travel of approximately 6 cm. Both stages have resolutions on the order of 10 μm, although the repeatability is considerably courser. For internal LIF measurements with the slotted insulator, the thruster was mounted on a platform supported by the axial translation stage and a linear ball bearing pillow block which provides unimpeded optical access.

Laser Induced Fluorescence

The experimental apparatus used for the laser induced fluorescence measurements consists of a tunable Coherent 899-21 single frequency titanium sapphire laser. The laser is actively stabilized to provide line widths on the order of 1 MHz with near zero frequency drift. Scan widths of up to 20 GHz can be realized at center wavelengths between 680 to 1060 nm. The titanium sapphire laser is pumped by Coherent solid state Verdi pump laser. The pump laser provides 5 W of single mode pump power at 532 nm. The laser wavelength was monitored by a Burliegh Instruments WA-1000 scanning Michaelson interferometer wavemeter with a resolution of 0.01 cm^{-1}. Figure 3 shows a schematic of the laser configuration.

The probe beam is directed into the Hall thruster plume by a series of mirrors. The slightly divergent beam (1.7 milliradians full angle) is focused to a submillimeter beam waist by a 50 mm diameter, 1.5 m focal length lens. For radial velocity measurements, the probe beam enters through a side window and is focused by a 50 mm diameter, 50 cm focal length lens. The collection optics for both radial and axial velocity measurements consist of a 75 mm diameter, 60 cm focal length, collimating lens. The collected light is then focused on to the entrance slit of a 0.5 m Ebert-Fastie monochrometer with a 50 mm diameter, 30 cm focal length, lens. An optical field stop is placed between

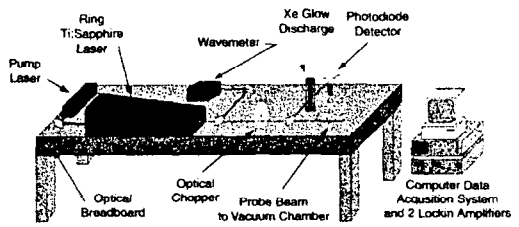

Fig. 3. LIF velocimetry apparatus with laser system and collection optics.

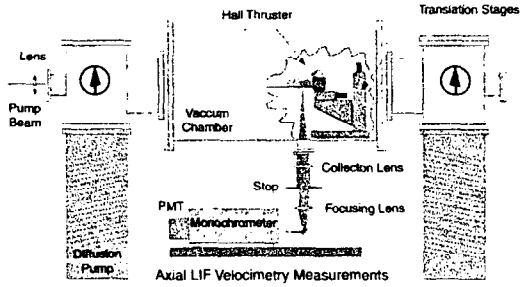

Fig. 4. Stanford high vacuum facility and LIF collection optics with cutaway view of Hall thruster.

the two lenses to match the F/# of the optical train with that of the monochrometer. A schematic of the collection optical train is shown in Fig. 4. The monochrometer is used as a narrow band optical filter so that only light from the transition of interest is collected. With entrance and exit slits full open (425 μm), the 600 groove/mm plane grating blazed for 600 nm within the monochrometer allows the Hamamatsu R928 photomultiplier tube (PMT) to sample a wavelength interval of approximately 1 nm. The orientation of the monochrometer allows the height of the slits to define the length of the probe beam along which the fluorescence is collected. The sample volume for all data presented in this work is approximately 100 μm in diameter and 2 mm in length. Prior to each test and with the PMT housing removed, a HeNe laser is reversed through the entire collection optical train to insure the alignment with the probe beam. For neutral LIF velocimetry measurements, a portion of the probe beam is split from the main beam, passed through a xenon glow discharge tube, and used as an stationary absorption reference. A silicon photodiode monitors the absorption signal. This use of the glow discharge tube is only possible for neutral xenon. The glow discharge does not support a sufficient population of excited state ions.

The LIF signal is collected using a Stanford Research Systems SRS-850 digital lockin amplifier. The probe bean is chopped by an SRS-540 optical chopper. The absorption signal from the stationary reference is collected using an SRS-530 lockin amplifier. Data from the absorption signal, laser power output, and the wavemeter are stored on the SRS-850 using 3 available analog inputs along with the LIF signal. Typical tests consist of a 12-20 GHz scan of the probe laser frequency over a 3 minute period. The beam is chopped at a frequency of 1.5 kHz. Both lockin amplifiers use 1 s time constants. Data is sampled at 8 Hz, producing four traces of approximately 2,000 points for each velocity data point. Several unsaturated traces using lower laser intensities, 10 s time constants, and 10 min scans were also performed.

Results and Analysis

Operating Conditions

The Hall thruster was operated at four conditions. At each of these conditions, the peak magnetic field was measured to be approximately 125 G, the mass flow to the anode was 2 mg/s, mass flow to the cathode was 0.3 mg/s. The test conditions corresponded to discharge voltages of 100, 160, 200, and 250 V. The anode currents for these conditions were 2.1, 2.4, 2.6, and 2.9 A, respectively. The total power consumed by the cathode and magnet circuit was approximately 30 W. It should be noted that the power dissipated in the ballast resistors on the anode and cathode keeper lines (~10 W) are not included in these calculations.

Position Reference

All spatially resolved measurements are referenced to a two coordinate system. The position in the radial coordinate is referenced to the difference of the radial location and the radial location corresponding to the acceleration channel center using the variable D which is defined as positive toward the thruster centerline. The axial coordinate is given by Z which is the distance from the thruster exit plane and is defined as positive along the thrust vector.

Saturation Study

The $5d[4]_{7/2} - 6p[3]_{5/2}$ ionic xenon transition at 834.7 nm was probed to extract local velocity data from the doppler shift of the measured fluorescence. Figure 5 shows the saturation curve of the transition at a location 13 mm from the exit plane and at the center of the acceleration channel. Here, the laser beam is propagating normal to the thrust vector and is measuring the radial velocity component of the xenon ions. A typical saturated

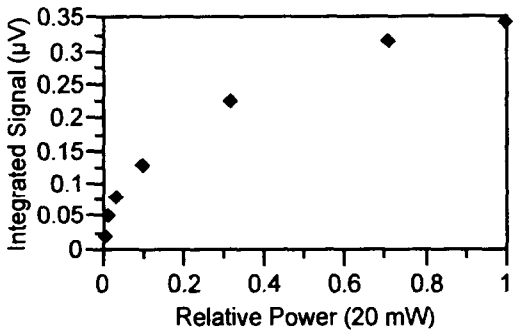

Fig. 5. Saturation curve of radial ionic measurements at Z = 13 mm and D = 0 mm.

trace used to determine the velocity in the probed volume is compared to an unsaturated trace from the same location in Fig. 6. Both traces are normalized to unity peak signal.

Velocity measurements for each of the saturated line shapes making up Fig. 5 are shown in Fig. 7. The mean velocity for this data points yields a value of -62 m/s with a standard deviation of 65 m/s and a range of 127 m/s. The absolute accuracy of the measurements is determined by the uncertainty of the wavelength meter and is taken to be ±500 m/s. The most important conclusion that can be drawn from this data is that the $5d[4]_{7/2} - 6p[3]_{5/2}$ ionic transition of xenon provides useful LIF velocimetry data when partially saturated which is within the uncertainties of the measurement of the Doppler shift. This allows the collection of saturated fluorescence signals, maximizing the signal to noise ratio and/or allowing for faster scans to be taken of the line while still being able to extract valuable velocity data from the acquired fluorescence signal. Similar results were obtained in a neutral saturation study.

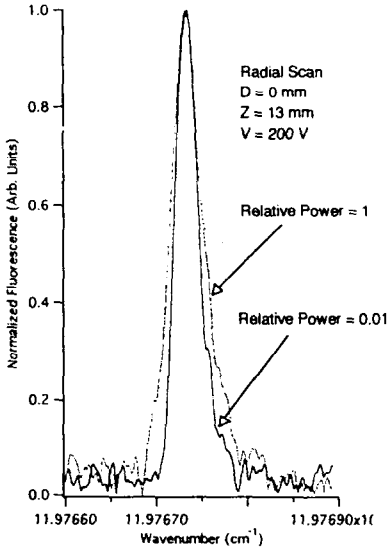

Fig. 6. Saturated and unsaturated ionic LIF traces

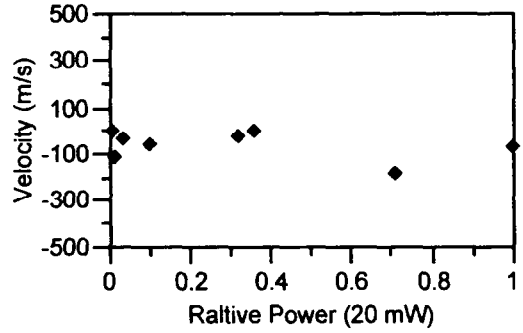

Fig. 7. Invariance of measured radial ionic velocity in saturation study.

Ionic LIF Velocimetry

The axial LIF velocimetry data consists of two sets of measurements taken with the slotted insulator. The first set consists of ionic velocity measurements taken externally extending from the exit plane to approximately Z = 35 mm. The second set of data points consist of internal axial velocity data from the exit plane to approximately Z = -65 mm. These limits are imposed by the limited range of the translation stage providing axial motion of the Hall thruster. Between each data set, the translation stages had to be repositioned so that the subsequent data set could be taken. Data points were taken every 2.5 mm with a sample probe volume 100 μm in diameter and 2 mm long. Overlap of the two data traces ensure that the measurements are continuous. For several of the test conditions examined, profiles of the axial velocity across the coordinate D are also examined.

The complete axial velocity profiles for the four cases examined are shown in Fig. 8. The error bars correspond to the uncertainty associated with the determination of the magnitude of the Doppler shift (500 m/s). The axial velocity profiles exhibit a typical behavior. The velocity is near zero near the anode (Z = -78 mm), and begins to rise near Z = -10 mm. The ions are rapidly accelerated in the region of the exit plane and reach their full velocity in the neighborhood of Z = 20 mm. This latter position corresponds to the location of the hollow cathode neutralizer relative to the body of the thruster and is often referred to as the *cathode plane* in the literature [17].

The length of the acceleration region for each case shown is invariant at 30 mm. Therefore, increases in the anode potential result in linearly increased electric fields within the thruster acceleration channel. The initial acceleration begins 10 mm within the thruster where the magnetic field has a value of approximately 85% of the centerline (D = 0) maximum. The propellant acceleration is completed 20 mm beyond the exit plane when the magnetic field has a value of approximately 25% of the centerline maximum.

Significant acceleration occurs outside the Hall thruster. Taking into account the uncertainties

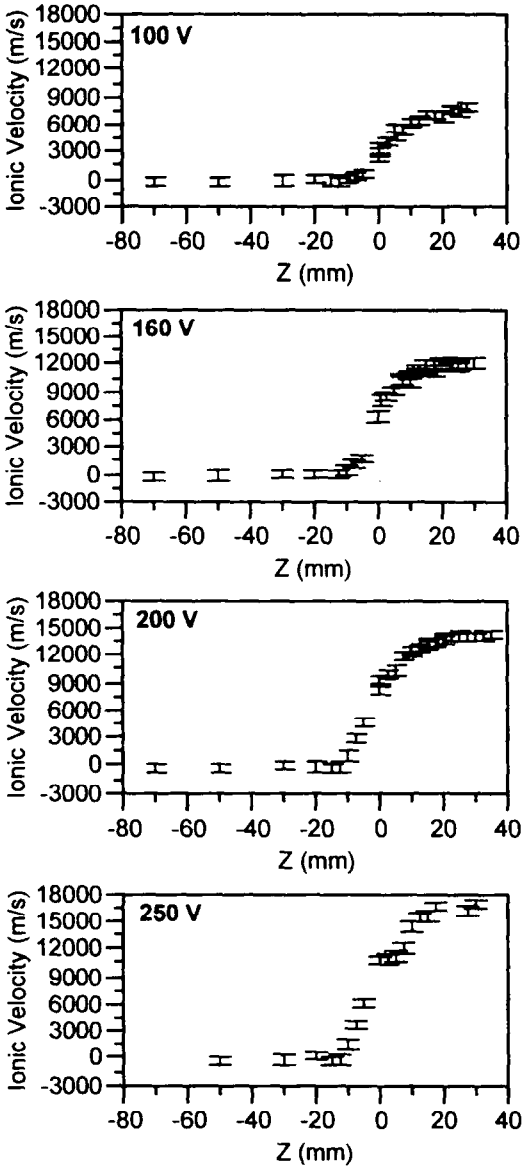

Fig. 8. Axial ionic velocity measurements at D = 0 mm for 4 discharge voltage conditions.

inherent to the velocity measurements (±500 m/s), the velocity increment imparted into the propellant outside the Hall thruster is essentially constant with an average value of 5,000 m/s. Only for the case of a 100 V discharge voltage, does the majority of the acceleration occur outside the thruster. Higher discharge voltages appear to have a constant percentage of the acceleration occurring externally. It is also informative to examine the energy deposited into the propellant. In the case of a 100 V discharge voltage, approximately 90% of the energy is deposited into the propellant beyond the exit plane. For all cases above 160 V discharge voltage, the fraction of energy deposition beyond the exit plane is nearer to 60%. Thus, the majority of the energy deposition into the Hall thruster propellant stream occurs outside the thruster body. However since the thrust is equivalent to the momentum flux, the majority (65%) of the thrust is still generated within the thruster body in all cases but that of the 100 V discharge voltage. In all the cases, approximately 60 eV appear to not contribute to the propellant acceleration. This value is constant to within the uncertainties of the velocity measurements and implies that the mechanism responsible for this loss is invariant with the applied anode potential. This energy loss is therefore most likely a product of the anode and cathode potential falls and other mechanisms inherent to the thruster design. It must be noted that the measurements presented thus far are limited to axial velocities and can not account for losses due to plume divergence.

Several radial profiles of the axial ionic velocity in Fig. 9 illustrate the radial variation of the measured axial velocities for a discharge voltage of 160 V at two locations in the plume and within the thruster for a discharge voltage of 200 V. The width of the acceleration channel is approximately 12 mm (-6 mm < D < 6 mm) and it is quite evident that the plume is sufficiently diverged at the axial locations examined such that the axial velocity profile is flat which strongly implies lines of constant potential in the radial direction.

Radial velocity measurements were performed in the plume. Combined with the above axial velocity measurements with the knowledge that the axial velocity appears to be independent of D, vector plots of the near plume may be constructed. Figure 10 shows a vector plot constructed for a 200 V discharge voltage. In this case, radial velocities vary linearly with D with near zero velocity at D = 0 mm and peak at values above 6,000 m/s

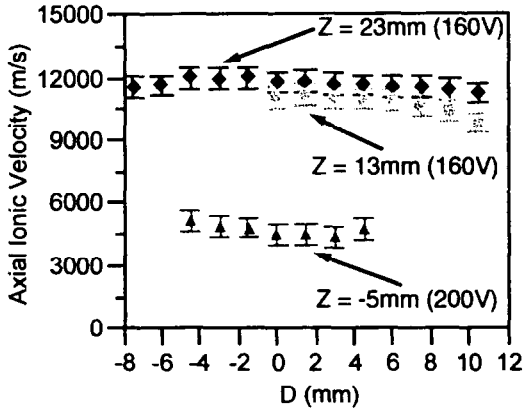

Fig. 9. Profiles of the axial ionic velocity for several discharge voltages and locations.

as close as Z = 13 mm and D = 8 mm. A strong feature of a Hall thruster plume is the central core of the plume. The propellant stream exits the thruster in an annulus, but a intense, optically emitting conical feature starting near the central magnetic core and extending a distance into the vacuum chamber is especially evident at higher discharge voltages and extends several meters in vacuum facilities with lower background pressures than those available at Stanford University. This inward focus of the divergent propellant flow likely accounts for this commonly observed plume structure.

Ionic Line Shape Analysis

The hyperfine splitting constants for the ionic xenon $5d[4]_{7/2} - 6p[3]_{5/2}$ transition at 834.7 nm are only known for the upper $6p[3]_{5/2}$ state. Similarly, the isotope shifts for this transition are unknown. In addition to the lack of spectroscopic information, the plasma environment introduces uncertainties in the determination of an ionic kinetic temperature from an unsaturated line shape. First, the time averaged broadening of the excitation spectra can not be due to plasma oscillations. King has shown in energy analyzer studies that the axial velocity of the exiting ions have an energy distribution of approximately 10 eV due to the plasma oscillations within the Hall thruster [26]. Second, the low density of the plasma may preclude a Maxwellian velocity distribution among the ions. If so, the concept of a kinetic temperature is not valid. The issue of the distribution of ionic velocities is minimized by examining the fluorescence spectra in the radial direction. The spectra is taken from the position with the minimum measured velocity, approximately 100 m/s at a location of D = 0 mm and Z = 13 mm. The ion population is assumed to be Maxwellian, or at least frozen into a close facsimile.

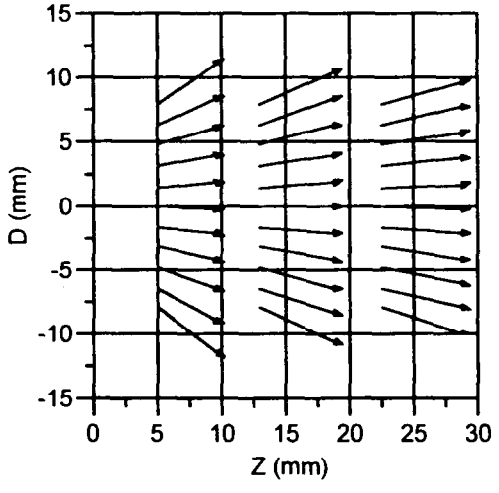

Fig. 10. Estimated flow vectors from radial velocity measurements for a 200 V discharge

Despite the inherent limitations, an estimate of the kinetic temperature is still possible if uncertainties of 40-70% are acceptable [27]. An unsaturated fluorescence trace is shown in Fig. 11 and compared to a model developed by Cedolin [28]. The model uses the $5d[3]_{7/2}$ lower level

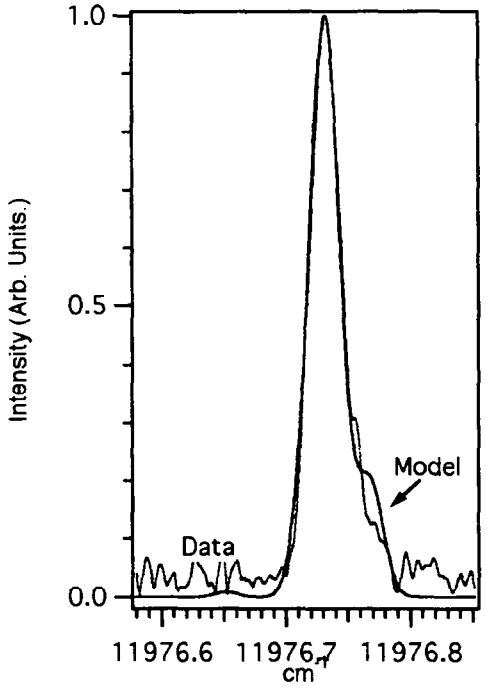

Fig. 11. Model fit to unsaturated fluorescence trace at 200 V, D = 0 mm, and Z = X mm.

hyperfine spin splitting and isotopic shift data from the 605.1 nm transition and the measured splitting data for the upper $6p[3]_{5/2}$ level. Lorentzian broadening is neglected and only Doppler broadening is considered. The best fit of this model predicts a kinetic temperature of approximately 450 K. The model still does not completely predict the outlying features, but this is expected since the incorrect spin splitting constants are used for the lower level. As a final note on the uncertainty of this model, if hyperfine splitting is ignored and only the isotope shifts corresponding to the values for the 605.1 nm transition are used, the model predicts a kinetic temperature of approximately 750 K.

The kinetic temperature of the ions is between 450 and 750 K. The uncertainty of this measurement is in large part due to the uncertainties of the spectral data as well as due to the noise in the fluorescence signal. A similar measurement in the plume of a SPT-100 by Manzella yielded a kinetic temperature of approximately 800 K [17]. It should be noted that Manzella used the incorrect value of J for the lower state which was first misidentified by Humphreys [29] and propagated by Moore [30] before finally being corrected by Hansen and Persson [18]. This may account for the slightly higher kinetic temperature; although, the uncertainty is such that the difference in the temperatures is probably inconsequential.

Neutral LIF Velocimetry

Figure 12 shows axial neutral velocity measurements within the acceleration channel of the Hall thruster. All four cases examined show very similar behavior. The initial velocity near the anode is very low. The neutral velocity slowly rises until a position approximately 20 mm within the thruster. At this point where the ion acceleration also begins, the neutrals are accelerated at a higher rate until near the exit plane where the acceleration appears to slow and even reverses when the thruster is operated at discharge voltages of 200 V, or above. The decrease in the neutral velocity is best explained by the thruster ingestion of background neutral xenon. Since the effect appears to grow with increased discharge voltage, it is possible that a portion of the flow reflected from nearby vacuum facility walls is ingested by the thruster. Once the background neutral xenon is in the vicinity of the discharge, the high electron density near the exit plane will collisionally excite the background atoms. Some of these atoms will be ionized and the external electric fields produced by the thruster will

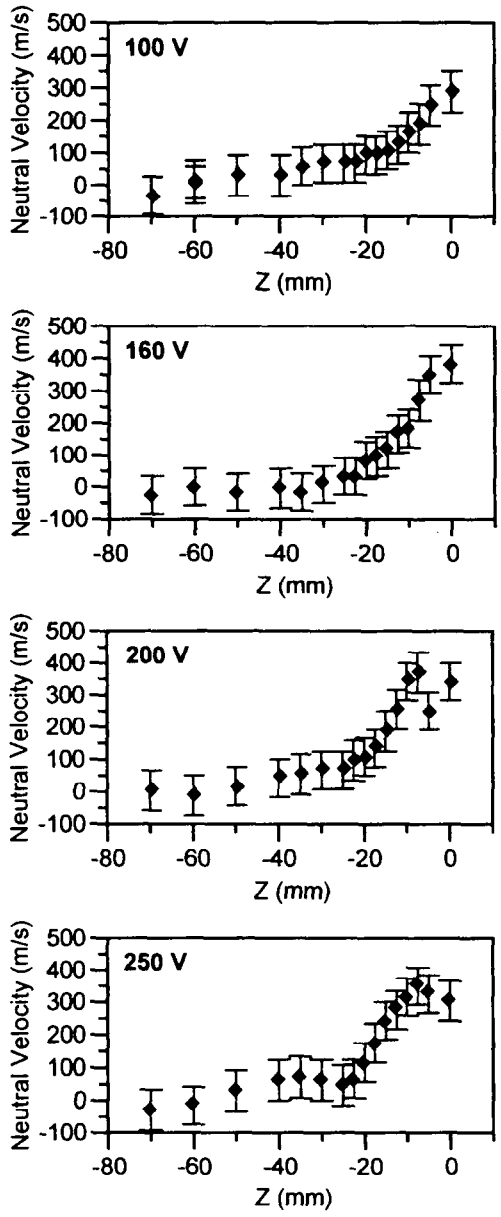

Fig. 12. Axial neutral velocity measurements at D = 0 mm for several conditions.

accelerate the resulting ions downstream, albeit with lower final energies than ions created within the thruster. Some of the atoms will be electronically excited, but not be ionized and will optically decay to the $6s[3/2]_2^0$ metastable level where they could be sampled during neutral LIF velocimetry measurements.

Flow from the cathode can be eliminated as the source of the apparent slowing down of the neutrals for several reasons. First, the flow from the cathode, although 15% of the anode flow, is exiting

from a 2 mm orifice approximately 12 cm above the sample volume. Flow from the cathode should be sufficiently diffused and not affect the neutral velocity measurements. Second, the cathode is angled 30° from the front plate pointed downstream. It is difficult to see how flow from the cathode could affect neutral velocity measurements within the acceleration channel. It is therefore almost certain that random neutral flux from the chamber background is responsible for the apparent drop in neutral velocity seen near the exit plane in Fig. 12.

Due to the highly nonequilibrium nature of the Hall thruster, it is important to understand the apparent acceleration of the neutrals. The plasma within the Hall thruster is required to be very diffuse by the constraint that the magnetic field restrain the electron flux to the anode. This requirement appears to be in force when the neutral velocity measurements are compared with the ionic velocity measurements. The disparate velocities of the ions and neutrals strongly suggest that the neutral and ion populations are not coupled. As such, the apparent acceleration of the neutrals may actually be an artifact of the time of flight of the neutrals through the volumetric zone of ionization. Slower neutrals, or neutrals that travel a longer effective path length due to collisions with the walls of the acceleration channel, have a proportionally greater chance being ionized than do neutrals in the high energy portion of the velocity distribution. Therefore, neutrals from the high energy tail of the velocity distribution are more likely to reach the upstream portions of the acceleration channel. In this case, there is no actual acceleration of the neutrals, but rather a depletion of the slower moving neutrals by ionization. This has been shown to be possible by integration of the Boltzmann equation [31].

Electric Field Calculations

The axial component of the electric field calculated by determining the ion kinetic energy from the velocimetry data in Fig. 8 and differentiating to produce an effective electric field as shown in Fig. 13. It is compared to electric field data calculated from emissive probe plasma potential measurements [8]. The two data sets show remarkable similarity indicating that the ionization and acceleration regions within the thruster are separated to some degree. The differences between the two sets of curves are due to the differences between the data. Ion creation occurs in a volume and therefore the LIF derived plasma potentials are only valid beyond the region of ion creation which appears to lie near Z = -10 mm. Unfortunately, there is probably some ionization occurring throughout the acceleration channel which accounts for some of the differences. Some ions are likely created in regions where the electric field is high and this masks the detection of local electric fields using velocimetry data, especially if the zone of ion creation is large and the ion velocities are subsequently distributed.

Another issue with determining plasma potentials and electric fields from velocimetry data is that the uncertainties associated with the ionic velocity measurements are magnified by the derivation of potential and subsequent electric field data. With the plasma potential probe, the primary issue is the degree of disturbance by the probe while the LIF velocimetry is non-intrusive, or less intrusive with the addition of the slot in the insulator.

Both data sets show similar trends. Some of the features are different, particularly those more than 10 mm within the Hall thruster exit plane. Between Z = -10 mm and the anode, there exists only a small population of ions with low axial velocities with uncertain creation and loss rates. Velocimetry studies prove inadequate to study the potential and electric field in this region, but potential probe measurements, assuming that they do not significantly perturb thruster operation, provide better measurement of the plasma potential and subsequently a better indication of the electric field. It is believed that the probe, undermeasures the higher gradients of the plasma potential due to the probe body perturbing the plasma flow field. This would explain the why the electric fields measured by the probe are somewhat less than those determined from velocimetry studies.

It is interesting to note that the trends of both measurements agree, particularly near the exit plane where a very low electric field is indicated. This sudden change in the electric field at the exit plane is visible in both data sets and increases with increasing discharge voltage. If it can be assumed that the axial current is a constant and since the local radial magnetic field is continuous, the dips in the electric field can be attributed to changes in the local plasma conductivity indicating either a sharp drop in the electron temperature, or a rise in the electron density. The measured electron temperature does not support the former; therefore, a sharp rise in the electron density may be responsible. The

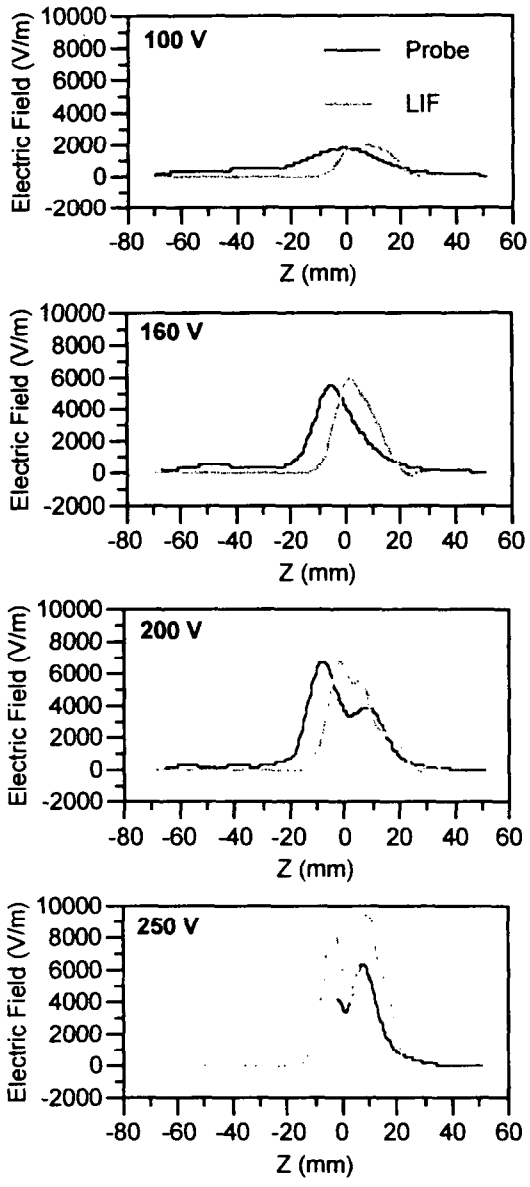

Fig. 13. Comparison of axial electric field calculated from plasma potential and LIF velocimetry data.

most likely explanation for a rise in electron density is that due to the high back pressure within the vacuum facility (10^{-4} Torr) there may be a second ionization zone near the exit plane of the thruster. In flowing electrons ionizing background neutrals could produce a higher plasma density in this region thus increasing the local plasma conductivity and lowering the local electric field as seen in Fig. 13. Alternatively, there may exist a region near the exit plane of increased plasma turbulence which may produce increased plasma conductivity.

Conclusions

Measurements of ion and neutral velocities were performed in the plume and into the interior of the thruster through a 1 mm wide slot in the outer insulator wall. From these measurements, information on propellant energy deposition, electric field strength, and flow divergence were extracted.

Ionic velocity measurements of axial velocity both inside and outside the thruster as well as radial velocity measurements outside the thruster, were performed using LIF with nonresonant signal detection using the ionic xenon $5d[4]_{7/2} - 6p[3]_{5/2}$ excitation transition while monitoring signal from the $6s[2]_{3/2} - 6p[3]_{5/2}$ transition. Neutral velocity measurements were similarly performed in the interior of the Hall thruster using the $6s[3/2]_2^0 - 6p[3/2]_2$ transition with resonance fluorescence collection. Most velocity measurements used saturated transitions to improve the signal to noise ratio. One radial trace of the ionic transition was taken in the linear fluorescence region and yielded an ionic translational temperature between 450 and 750 K. However, since the hyperfine structure constants are not known for the $5d[4]_{7/2}$ level, the constants for the $5d[3]_{7/2}$ level were used instead. This result should therefore be viewed with caution. The ionic velocity data allowed for the measurement of the energy deposited into the propellant stream which was calculated as the kinetic energy of the ions. An effective electric field was calculated from the ionic kinetic energy. Electric field values derived from the ion velocity measurements show that the fields are relatively smooth and peak near the exit plane. Maximum field strengths were found to be approach 8,000 V/m. At the exit plane, the axial electric fields show a dip for nearly all the discharge voltages examined.

Acknowledgments

This work is supported by the Air Force Office of Scientific Research. W.A. Hargus, Jr. was supported under the Air Force Palace Knight Program.

References

1. S.W. Janson, "The On-Orbit Role of Electric Propulsion," AIAA-93-2220, 29th Joint Propulsion Conference, 28-30 June 1993, Monterey, CA.

2. R.J. Cedolin, W.A. Hargus, Jr., R.K. Hanson, and M.A. Cappelli, "Laser Induced Fluorescence Diagnostics for

Xenon Hall Thrusters," AIAA-96-2986, 32nd Joint Propulsion Conference, July 1-3, 1996, Lake Buena Vista, FL.

3. R.J. Cedolin, W.A. Hargus, Jr., R.K. Hanson, and M.A. Cappelli, "Laser Induced Study of a Xenon Hall Thruster," AIAA-97-3053, 33rd Joint Propulsion Conference July 6-9, 1997, Seattle, WA.

4. W.A. Hargus, Jr., N.B. Meezan, and M.A. Cappelli, "Transient Behavior of a Low Power Hall Thruster," AIAA-97-3050, 33rd Joint Propulsion Conference July 6-9, 1997, Seattle, WA.

5. W.A. Hargus, Jr., R.J. Cedolin, N.B. Meezan and M.A. Cappelli, "A Performance Study of a Low Power Hall Thruster," AIAA 97-3081, 33rd Joint Propulsion Conference July 6-9, 1997, Seattle, WA.

6. R.J. Cedolin, W.A. Hargus, Jr., P.V. Storm, R.K. Hanson, and M.A. Cappelli, "Laser-induced Fluorescence Study of a Xenon Hall Thruster, *Applied Physics B: Lasers and Optics*, Vol. 65, pp 459-469, 1997.

7. W.A. Hargus, Jr. and M.A. Cappelli, "Laser Induced Fluorescence Measurements on a Laboratory Hall Thruster," AIAA-98-3645, 34th Joint Propulsion Conference, 13-15 July 1998, Cleveland, OH.

8. W.A. Hargus, Jr. and M.A. Cappelli, "Interior and Exterior Laser-induced Fluorescence and Plasma Potential Measurements on a Laboratory Hall Thruster," AIAA-99-2721, 35th Joint Propulsion Conference, 20-24 June, 1999, Los Angeles, CA.

9. P.V. Storm, *Optical Investigations of Plasma Properties in the Interior of a Arcjet Thrusters*, Thermosciences Division Report No. TSD-102, Ph.D. Dissertation, Stanford University, 1997.

10. R. P. Lucht, "Applications of Laser-Induced Fluorescence Spectroscopy," in *Laser Spectroscopy and its Applications*, edited by L. J. Radziemski, R. W. Solarz, and J. A. Paisner, Marcel Dekker, New York, 1987.

11. A.C. Eckbreth, *Laser Diagnostics for Combustion Temperature and Species*, Overseas Publishers Association, Amsterdam, 1996.

12. W. Demtroder, *Laser Spectroscopy: Basic Concepts and Instrumentation*, Springer-Verlag, Berlin, 1996.

13. G. Herzberg, *Atomic Spectra and Atomic Structure*, Dover Publications, New York, 1944.

14. R. D. Cowan, *The Theory of Atomic Structure and Spectra*, University of California Press, Berkley, California, 1981.

15. I. I. Sobelman, *Atomic Spectra and Radiative Transitions*, Springer-Verlag, New York, 1992.

16. H. E. White, *Introduction to Atomic Spectra*, McGraw-Hill Book Co., New York, 1934.

17. D.H. Manzella, "Stationary Plasma Thruster Ion Velocity Distribution," AIAA-94-3141, 30th Joint Propulsion Conference, June 27-29, 1994, Indianapolis, IN.

18. J. E. Hansen and W. Persson, "Revised Analysis of Singly Ionized Xenon, Xe II," *Physica Scripta*, Vol. 36, pp 602-643, 1987.

19. D. R. Lidde, Ed., *Handbook of Chemistry and Physics*, CRC Press, Inc., Boca Raton, Florida, 74th Edition, 1993.

20. D. A. Jackson and M. C. Coulombe, "Isotope Shifts in the Arc Spectrum of Xenon," *Proc. R. Soc. Lond. A.*, Vol. 338, pp 277-298, 1974.

21. G. Borghs, P. De Bisschop, R. E. Silerans, M. Van Hove, and J. M. Van den Cruyce, "Hyperfine Structures and Isotope Shifts of the $5d\,^4D_{7/2} \rightarrow 6p\,^4P^0_{5/2}$ Transition in Xenon Ions," *Atoms and Nuclei*, Vol. 299, pp 11-13, 1981.

22. C. R. Bingham, M. L. Gaillard, D. J. Pegg, H. K. Carter, R. L. Mlekodaj, J. D. Cole, and P. M. Grffin, "Colinear Fast-Beam laser Spectroscopy Experiment: Measurement of Hyperfine Structure and Isotope Shifts in Xe II," *Nuclear Instruments and Methods*, Vol. 202, pp 147-152, 1982.

23. H. Geisen, T. Krumpelmann, D. Neuschafer, and Ch. Ottinger, "Hyperfine Splitting Measurements on the 6265 Å and 6507 Å Lines of Seven Xe Isotopes by LIF on a Beam of Metastable $Xe(^3P_{0,3})$ Atoms," *Physics Letters A*, Vol. 130, No. 4.5, 11 July 1988.

24. W. Fischer, H. Huhnermann, G. Kromer, and H.J. Schafer, "Isotope Shifts in the Atomic Spectrum of Xenon and Nuclear Deformation Effects," *Z. Physik*, Vol. 270, No. 113, 1974.

25. L. Bronstrom, A. Kastberg, J. Lidberg, S. Mannervik, "Hyperfine-structure Measurements in Xe II," *Physical Review A*, Vol. 35, No. 1, Jan. 1996.

26. L. B. King, *Transport-Property and Mass Spectral Measurements in the Plasma Exhaust Plume of a Hall-Effect Space Propulsion System*, Ph.D. Dissertation, Aerospace Engineering, University of Michigan, June 1998.

27. R. J. Cedolin, Personal Communication, 23 Jan. 1999.

28. R. J. Cedolin, *Laser-Induced Fluorescence Diagnostics of Xenon Plasmas*, Ph.D. Dissertation, Mechanical Engineering, Stanford University, June 1997.

29. C. J. Humpreys, "Second Spectrum of Xenon," *Journal of the National Bureau of Standards*, Vol. 22, Jan. 1939.

30. C. E. Moore, *Atomic Energy Levels: Volume III*, National Bureau of Standards, Washington, 1958.

31. J. M. Fife, Personal Communication, 23 June 1999.